NASA Contractor Report 198452

Numerical Investigation of Two-Phase Flows With Charged Droplets in Electrostatic Field

Sang-Wook Kim
Thermoscience Research Corp.
Brook Park, Ohio

February 1996

Prepared for
Lewis Research Center
Under Contract NAS3–78048–D

National Aeronautics and
Space Administration

Numerical investigation of two-phase flows with charged droplets in electrostatic field

Sang-Wook Kim
Thermoscience Research Corp.
Brook Park, Ohio 44142

Prepared for
NASA Lewis Research Center
Under Contract C-78048-D

ABSTRACT

A numerical method to solve two-phase turbulent flows with charged droplets in electrostatic field is presented. The ensemble-averaged Navier-Stokes equations and the electrostatic potential equation are solved using a finite volume method. The transitional turbulence field is described using multiple-time-scale turbulence equations. The equations of motion of droplets are solved using a Lagrangian particle tracking scheme, and the inter-phase momentum exchange is described by the Particle-In-Cell scheme. The electrostatic force caused by an applied electrical potential is calculated using the electrostatic field obtained by solving a Laplacian equation and the force exerted by charged droplets is calculated using the Coulombic force equation. The method is applied to solve electro-hydrodynamic sprays. The calculated droplet velocity distributions for droplet dispersions occurring in a stagnant surrounding are in good agreement with the measured data. For droplet dispersions occurring in a two-phase flow, the droplet trajectories are influenced by aerodynamic forces, the Coulombic force, and the applied electrostatic potential field.

NOMENCLATURE

$A_{i,p}$ coefficient for $i-th$ velocity component at a grid point p

b vector of body force ($=\{b_x, b_r\}$)

c_μ eddy viscosity coefficient

$c_{\mu f}$ constant coefficient (=0.09)

d_ℓ diameter of a droplet

F_i inter-phase force $[Kg/(m^2 \cdot \sec^2)]$, $i=\{x,r\}$

f_a aerodynamic force

f_C Coulombic force

f_{ES} electrostatic force caused by applied electrical field

h distance from meniscus to collecting surface

k turbulent kinetic energy ($=k_p+k_t$)

k_p turbulent kinetic energy in production range

k_t turbulent kinetic energy in dissipation range

m_ℓ mass of a droplet

N_d number of particles or droplets

P_r production rate

p pressure

$p*$ initial guess for pressure

$p**$ corrected pressure

p' incremental pressure

q_j charge of a droplet

$R_{e\ell}$ droplet Reynolds number, $R_{e\ell}=\rho|\tilde{\mathbf{v}}-\mathbf{v}_\ell|d_\ell/\mu$

r_ℓ radius of a droplet

U_e external free stream velocity

U_o initial velocity of air jet

u_j^* initial guess for velocity

u_j^{**} predicted velocity

u_j^{***} corrected velocity

$\tilde{\mathbf{v}}$ ensemble averaged, gas phase velocity vector, $\tilde{\mathbf{v}} = \{\tilde{u}_j | j=1,2\} = \{\tilde{u}, \tilde{v}\}$

$\mathbf{v}_\ell$ velocity vector for a droplet, $\mathbf{v}_\ell = \{u_{\ell,j} | j=1,2\} = \{u_\ell, v_\ell\}$

$\mathbf{x}$ spatial coordinates $(= \{x, r\})$

Δt time-step size for numerical integration

ε_ϕ permittivity of free space

ε_p energy transfer rate

ε_t dissipation rate

ϕ electrostatic potential field

μ molecular viscosity

μ_e effective viscosity $(= \mu + \mu_t)$

μ_t turbulent viscosity

ρ density of gas phase

Superscripts

n time-level for unsteady cases

Subscripts

e external boundary

f continuous gas phase

ℓ liquid droplets

o initial conditions

$\overline{(\,)}$ average value

1. Introduction

In electrohydrodynamic (EHD) sprays, dispersion of particles or droplets is caused by electrical force and aerodynamic force. Application of EHD sprays can be found in spray paintings, aerosols, fabrication of solar panels, and dust collecting mechanisms. The use of electrical force also offers the possibility of controlling dispersion of liquid fuel droplets in combustors and aerospace propulsion systems. A number of experimental and theoretical investigations have been made during past decades on two-phase flows for applications in combustors and aerospace propulsion systems. However, only a limited amount of research efforts have been made for two-phase flows with a charged discrete phase. Certainly, more experimental and theoretical research efforts will be made in the future to optimize dispersion of particles or droplets in various engineering applications. A few experimental and theoretical works closely related to the present work are discussed below.

Experimental data on electrostatic spray emitted from a meniscus used in the present work can be found in ref. [1]. Subsequently, the experimental case was studied numerically by Ganan-Calvo et al. [2] using a Lagrangian particle tracking technique. The charged droplets emanating from the meniscus are accelerated by an applied electric potential and by an air jet surrounding the meniscus [3]. However, detailed data on the air jet are not available. In the work of Ganan-Calvo et al., the aerodynamic force acting on a droplet was calculated assuming that the surrounding air is in a stagnant state. Numerical droplets are seeded at locations 60~80 droplet radii downstream of the conical meniscus. Their calculated velocity profiles are in good agreement with measured data. The good comparison between the calculated results and the measured droplet velocity profiles indicates that the influence of the airflow on the droplet motion is negligibly small. Experimental investigations on dispersion of chemically reacting, charged droplets have also

appeared in recent years [4]. However, detailed measured data for two-phase turbulent flows with charged discrete phase are still very scarce.

In gas-droplet two-phase flows, inter-phase mass, momentum, and energy exchanges exist. For the two-phase flow considered herein, the influence of evaporation of liquid droplets on the gas phase is negligible since the time interval that droplets are exposed to airflow is very small. Also, energy exchange is ignored since the fluid flow is in an isothermal state. In the present numerical investigation, the inter-phase momentum exchange is resolved using the particle-in-cell (PIC) scheme of Crowe et al. [5]. Implementation of the PIC is described in more detail in the "Numerical methods" section.

The numerical method used in this work is a pressure-based Navier-Stokes equations solver that incorporates a pressure-staggered mesh and an incremental pressure equation for the conservation of mass. The accuracy of the numerical method has been validated by solving a number of flow cases. Calculations of two-dimensional self-sustained oscillatory flows over a circular cylinder and a square cylinder can be found in ref. [6], and calculations of three-dimensional lid-driven cavity flow and a laminar flow through a curved duct can be found in ref. [7]. Further application of the numerical method for various laminar flows, complex turbulent flows, incompressible flows, compressible flows, steady flows, unsteady flows, and chemically reacting flows can be found in refs. [8-11] and the references cited therein.

It has been shown that the multiple-time-scale (M-S) turbulence equations used in this work yield accurate numerical results for various complex turbulent flows. The numerical results for various incompressible and compressible turbulent flows (e.g., an unsteady transitional flow over an oscillating airfoil, circular jets in crossflow, transonic flows with shock wave - boundary layer interactions, a confined swirling jet, and divergent channel flows) obtained using the M-S

equations are in as good agreement with the measured data as those obtained using optimized k-ε turbulence models, algebraic Reynolds stress turbulence models (ARSM), or Reynolds stress turbulence models (RSM) for each flow case. It has also been shown that the M-S equations can resolve ignition delay, flame thickness, and chemical reaction - turbulence interaction occurring in a compressible shear layer [8]. It can be found in ref. [8] that the distribution of chemical species obtained using the M-S equations are in much closer agreement with the measured data than those obtained using $k-\varepsilon$ turbulence equations or a Monte-Carlo probability density function method. The physical aspects of the M-S equations are briefly discussed in this paper.

2. Theoretical Analysis

The mathematical equations governing an unsteady, two-phase, turbulent flows with a charged discrete phase include: the Navier-Stokes equations, turbulence equations, Lagrangian equations of motion for discrete phase, the Coulombic force equation, and an electrostatic potential equation. These equations are discussed below.

Conservation equations for gas phase flow

The electrostatic force acting on a droplet is contributed by the applied electrostatic potential and by charged droplets. The spatial location of each charged droplet is a function of time and, hence, a time-accurate solution technique needs to be used to solve two-phase turbulent flows with charged droplets. The ensemble-averaged conservation of mass equation is given as

$$\frac{\partial}{\partial x}(\rho\tilde{u})+\frac{1}{r}\frac{\partial}{\partial r}(r\rho\tilde{v})=0. \tag{1}$$

where ρ is the density and $\{\tilde{u},\tilde{v}\}$ are the ensemble-averaged velocities.

The ensemble averaged conservation of linear momentum equations in axisymmetric coordinates are given as

$$\frac{\partial}{\partial t}(\rho\tilde{u})+\frac{\partial}{\partial x}(\rho\tilde{u}\tilde{u})+\frac{1}{r}\frac{\partial}{\partial r}(r\rho\tilde{u}\tilde{v}) = \frac{\partial}{\partial x}\left\{2\mu_e\frac{\partial\tilde{u}}{\partial x}\right\}+\frac{1}{r}\frac{\partial}{\partial r}\left\{r\mu_e\left(\frac{\partial\tilde{u}}{\partial r}+\frac{\partial\tilde{v}}{\partial x}\right)\right\}-\frac{\partial\tilde{p}}{\partial x}+F_x \qquad (2)$$

$$\frac{\partial}{\partial t}(\rho\tilde{v})+\frac{\partial}{\partial x}(\rho\tilde{u}\tilde{v})+\frac{1}{r}\frac{\partial}{\partial r}(r\rho\tilde{v}\tilde{v}) = \frac{\partial}{\partial x}\left\{\mu_e\left(\frac{\partial\tilde{u}}{\partial r}+\frac{\partial\tilde{v}}{\partial x}\right)\right\}+\frac{1}{r}\frac{\partial}{\partial r}\left\{r\left(2\mu_e\frac{\partial\tilde{v}}{\partial r}\right)\right\}-\frac{\partial\tilde{p}}{\partial r}+F_r \qquad (3)$$

where $\tilde{p}$ is the ensemble-averaged pressure, $\{F_x, F_r\}$ is the inter-phase force, $\mu_e=\mu+\mu_t$ is the effective viscosity, and μ and μ_t are the molecular and turbulent viscosities, respectively. A numerical procedure for the inter-phase momentum exchange term is described later in the "Numerical methods" section.

Multiple-time-scale turbulence equations

The M-S equations are based on a simplified split-spectrum method [10]. In the method, the turbulent kinetic energy is split into turbulent kinetic energy in the low frequency range (k_p) and that in the high frequency range (k_t). Recall that the energy-containing eddies are generated by the instability of the mean fluid flow, the energy-containing eddies cascade to finer eddies, and the fine scale eddies are dissipated by the viscous force. Hence, the energy containing eddies are characterized by low frequencies and large values of k_p/k_t and the fine scale eddies are characterized by higher frequencies and small values of k_p/k_t. The capability to resolve the cascade is achieved by solving the convection-diffusion equations for the spectrum-split turbulent kinetic energies. Obviously, single-time-

scale turbulence models can not resolve the cascade of turbulent kinetic energy since spectrum-split turbulence quantities are not solved for in these turbulence models [10].

In complex turbulent flows, the production rate (P_r) and dissipation rate (ε_t) of the turbulent kinetic energy vary widely in space so that the shape and the frequency domain of the spectral density also vary widely in space. Such a state of turbulence is called "nonequilibrium turbulence." The capability to resolve the nonequilibrium turbulence phenomena originates from describing the turbulence length scale and the turbulent viscosity using the energy transfer rate (ε_p). In the M-S equations [10], the eddy viscosity coefficient that depends on the strength of nonequilibrium turbulence is given as;

$$C_\mu = C_{\mu f}\, \varepsilon_t / \varepsilon_p \tag{4}$$

where $C_{\mu f}$ is a constant coefficient. A few experimental and theoretical investigations on the dependence of the eddy viscosity coefficient on P_r/ε_t can be found in refs. [12-14]. In single-time-scale turbulence models, the turbulence length scale is defined using the dissipation rate and, hence, these turbulence models can not resolve the nonequilibrium turbulence phenomena.

Lagrangian description of droplet equations of motion

The Lagrangian equations of motion for discrete phase are given as [5, 15-17];

$$\frac{d\mathbf{x}_\ell}{dt} = \mathbf{v}_\ell \tag{5}$$

$$m_\ell \frac{d\mathbf{v}_\ell}{dt} = \mathbf{F}_\ell \tag{6}$$

where m_ℓ is the mass of a droplet, $\mathbf{F}_\ell = \frac{1}{2} c_d \rho |\tilde{\mathbf{v}} - \mathbf{v}_\ell| (\tilde{\mathbf{v}} - \mathbf{v}_\ell) \pi r_\ell^2 + \mathbf{b}$ is the sum of the aerodynamic force and the electrostatic force, πr_ℓ^2 is the wetted area of a droplet, and $\mathbf{b}$ is the electrostatic force. The drag coefficient is given as

$$c_d = \frac{24}{R_{e\ell}} \left(1 + \frac{1}{6} R_{e\ell}^{2/3} \right) \tag{7}$$

where the droplet Reynolds number is defined as

$$R_{e\ell} = \frac{\rho |\tilde{\mathbf{v}} - \mathbf{v}_\ell| d_\ell}{\mu} \tag{8}$$

The body force acting on a charged droplet in electrostatic potential field is given as

$$\mathbf{b}_j = \begin{Bmatrix} b_x \\ b_r \end{Bmatrix} = -q_j \nabla \phi + \sum_{\substack{k=1 \\ k \neq j}}^{N_d} \frac{1}{4\pi\varepsilon_\phi} \frac{q_j q_k}{R_{jk}^3} \mathbf{R}_{jk} \tag{9}$$

where q_j is the charge of a droplet, ϕ is the electrostatic potential field, N_d is the number of charged particles or droplets in the flow field, ε_ϕ is the permittivity of free space, $\mathbf{R}_{jk} = \mathbf{x}_j - \mathbf{x}_k$ and $R_{jk} = |\mathbf{R}_{jk}|$. For the class of problems considered in this study, the applied electrostatic field is in a steady state and the governing partial differential equation is given as [18];

$$\nabla^2 \phi = 0. \tag{10}$$

3 Numerical Method

The unsteady gas phase equations are solved using a finite volume method. In

the method, the velocities and turbulence quantities are located at the grid points and the pressure and the electrostatic potential are located at the centroid of a cell formed by the four adjacent velocity grid points. Interaction between the isothermal continuous gas phase and the discrete droplet phase are accounted for by considering the inter-phase exchanges of momentum. The transient solution for the gas phase is obtained by solving the flow equations iteratively at each time-level. The numerical method for the gas phase equations that include the inter-phase source term, particle equations of motion, and the applied electrostatic potential field are described below.

Numerical method for gas phase equations

The numerical method is a pressure based Navier-Stokes equations solver in which the predicted velocity is obtained by solving the momentum equations and the divergence free, corrected velocity is obtained by solving an incremental pressure equation derived from the conservation of mass equation.

Let $\tilde{u}_i^*$ and $\tilde{p}^*$ be the initial guesses for the velocity and pressure for a new time-level, respectively. Applying a finite volume method [6-11] to the momentum equations yields

$$\left(\rho C_1 + A_{i,p}^*\right)\tilde{u}_{i,p}^{**} = \sum_{k=1}^{nb} A_{i,k}^* \tilde{u}_{i,k}^{**} - \frac{\partial \tilde{p}^*}{\partial x_i}\Delta V + \rho C_2 \tilde{u}_{i,p}^{n-1} + S_i^* + S_{Fi}^* \qquad (11)$$

where $C_1 = C_2 = \int_{\Delta V} \frac{1}{\Delta t_f} d\mathbf{x}$, ΔV is the volume of a cell, $\Delta t_f = t^n - t^{n-1}$ is the time-step size, n denotes the time-level, nb is the number of neighboring grid points, $A_{i,p}^*$ is determined from the power-law upwind differencing scheme, S_i^* represents source terms contributed by non-orthogonal mesh and other velocity components, and S_{Fi}^* represents the inter-phase source term. The predicted

velocity, u_i^{**}, is obtained by solving eq. (11).

The inter-phase momentum transfer from the discrete phase toward the gas phase is contributed by gain or loss of momentum of the discrete phase. In the context of the PIC scheme, the inter-phase source term for the discrete momentum equation for each cell is obtained by summing up the source terms contributed by all the droplets inside the cell.

$$S_{Fi}^{*} = \frac{1}{\Delta t_f}\int_{t=t^n}^{t=t^{n+1}}\int_{\Delta V} F_i \, d\mathbf{x}dt$$

$$= \frac{1}{\Delta t_f}\sum_{k=1}^{N_C}\left[\int_{t=t^n}^{t=t^{n+1}}\left\{\frac{1}{2}c_d\rho\left|\tilde{\mathbf{v}}-\mathbf{v}_\ell\right|\left(\tilde{u}_i-u_{\ell,i}\right)\pi r_\ell^2\right\}_k dt\right] \tag{12}$$

where $u_{\ell,i}$ is the droplet velocity in the $i-th$ coordinate direction.

The predicted velocity field does not satisfy the conservation of mass until the solutions are fully converged. The corrected velocity and pressure that satisfy the conservation of mass and the momentum equations can be written as

$$\left.\begin{aligned}\tilde{u}_i^{***} &= \tilde{u}_i^{**} + \tilde{u}_i'\\ \tilde{p}^{**} &= \tilde{p}^{*} + \tilde{p}'\end{aligned}\right\}. \tag{13}$$

Then the corrected discrete momentum equation can be written as

$$\left(\rho C_1 + A_{i,p}^{*}\right)\tilde{u}_{i,p}^{***}$$

$$= \sum_{k=1}^{nb} A_{i,k}^{*}\tilde{u}_{i,k}^{***} - \frac{\partial(\tilde{p}^{*}+\tilde{p}')}{\partial x_i}\Delta V + \rho C_2 \tilde{u}_{i,p}^{n-1} + S_i^{*} + S_{Fi}^{*} \tag{14}$$

The inter-phase source term is not updated during the iterative solution process of the gas phase equations. Therefore, the time-step size of the gas phase for two-phase unsteady flows needs to be much smaller than that for single phase unsteady flows. Otherwise, the inter-phase momentum transfer may not be resolved accurately. Subtracting eq. (11) from eq. (14) yields the relationship between the incremental velocity and the incremental pressure given as

$$\tilde{u}_i' = -A_{u_i}\frac{\partial \tilde{p}'}{\partial x} \tag{15}$$

where $A_{u_i} = \Delta V/(\rho C_1 + A_{i,p}^*)$, and the contributions made by neighboring grid points have been disregarded. However, this simplification does not incur any mass imbalance in the converged solution since the incremental pressure is driven only by the mass imbalance as shown below.

The incremental pressure equation is obtained by inserting eq. (13) into eq. (1) and is given as, after some rearrangement,

$$-\frac{\partial}{\partial x}\left\{\rho A_u \frac{\partial \tilde{p}'}{\partial x}\right\} - \frac{1}{r}\frac{\partial}{\partial r}\left\{r\rho A_v \frac{\partial \tilde{p}'}{\partial r}\right\} = -\left\{\frac{\partial}{\partial x}\left(\rho \tilde{u}^{**}\right) + \frac{1}{r}\frac{\partial}{\partial r}\left(r\rho \tilde{v}^{**}\right)\right\} \tag{16}$$

where the right hand side represents the mass imbalance and is identical to the original conservation of mass equation. Therefore, the incremental pressure is driven only by the mass imbalance and the simplifications introduced during derivation of the incremental pressure equation do not incur any mass imbalance in the converged solution.

Applying the finite volume method to eq. (16) yields

$$A_p \tilde{p}_p' = \sum_{k=1}^{nb} A_k \tilde{p}_k' - \oint \bar{\rho}^* \tilde{u}_j^{**} n_j ds \tag{17}$$

where ds is the boundary surface of a pressure control volume. The incremental pressure is obtained by solving eq. (17), the incremental velocity is calculated using eq. (15), and the corrected velocity and pressure are calculated using eq. (13).

The turbulence equations are solved by the same finite volume method. At each time-level, the conservation of momentum equation, the incremental pressure equation, and the turbulence equations are solved iteratively until the velocity and pressure satisfy the prescribed convergence criterion. In principle, the incremental pressure equation needs to be solved iteratively until the residual term vanishes and, in such a case, the converged solution satisfies the conservation of mass and momentum equations exactly within the context of the difference approximation.

Particle Equations of Motion

The particle equations of motion are integrated using the Crank-Nicholson scheme. Let Δt_ℓ be the time-step size for the discrete phase. Then eqs. (5) and (6) can be written as;

$$\frac{\mathbf{x}_\ell^n - \mathbf{x}_\ell^{n-1}}{\Delta t_\ell} = \frac{1}{2}\mathbf{v}_\ell^{n+1/2} \tag{18}$$

$$m_\ell \frac{\mathbf{v}_\ell^n - \mathbf{v}_\ell^{n-1}}{\Delta t_\ell} = \frac{1}{2}\mathbf{F}_\ell^{n+1/2} \tag{19}$$

Eqs. (18) and (19) form a set of nonlinear equations since $\mathbf{F}_\ell$ depends on the droplet velocity as well as the gas-phase velocity that is a function of the spatial location. Ideally, eqs. (18) and (19) needs to be solved iteratively. Instead, a very small time-step size can be used to semi-implicitly integrate eqs. (18) and (19). The particle velocity and the force on the right hand side of eqs. (18) and (19) are calculated using

$$\left.\begin{aligned} \mathbf{v}_\ell^{n+1/2} &= \frac{1}{2}\left(\mathbf{v}_\ell^{n-1} + \mathbf{v}_\ell^{n}\right) \\ \mathbf{F}_\ell^{n+1/2} &= \frac{1}{2}\left(\mathbf{F}_\ell^{n-1} + \mathbf{F}_\ell^{n}\right) \end{aligned}\right\} \tag{20}$$

where $\mathbf{v}_\ell^n$ and $\mathbf{F}_\ell^n$ are evaluated using an explicit time-integration scheme. In gas-liquid two-phase flows, the physical time-scales as well as the numerically stable time-step-sizes for the continuous and the discrete phases are quite different. The use of a very small time-step size is necessary to accurately resolve the inter-phase momentum transfer. A very small time-step size also needs to be used for numerical stability. The use of a time-step size approximately two orders of magnitude smaller than that of the continuous phase yields stable and strongly convergent results. A similar conclusion can also be found in Raju and Sirignano [17].

The electrostatic force acting on a charged droplet is caused by the applied electrostatic potential field and by the Coulombic force acting among charged droplets. The force exerted by the applied electrical field is calculated using the electrical potential field obtained by solving a Laplacian equation. In numerical calculation, the electrical potential is defined at the center of a cell and the Laplacian equation is solved using the same procedure as that for the incremental pressure equation [6-11]. The force exerted by charged droplets is calculated directly using the Coulombic force equation.

The liquid spray is represented by a finite number of droplets with different size groups. Let $\dot{M}_{\ell,k}$ be the mass flow rate of the droplets in the $k-th$ size group. Then the total mass flow rate, $\dot{M}_\ell$, of the droplets is given as

$$\dot{M}_\ell = \sum_{k=1}^{N_{siz}} \dot{M}_{\ell,k} \tag{21}$$

where N_{siz} represents the number of all droplet size groups. The number flow rate of the physical droplets in the $k-th$ size group is given as

$$\dot{\eta}_k = \frac{\dot{\mathcal{M}}_{\ell,k}}{\frac{4}{3}\pi\rho_\ell {r_{\ell,k}}^3} \tag{22}$$

The number of physical droplets for each size group to be introduced at each time-level of the discrete phase is given as

$$N_k^n = \dot{\eta}_k \Delta t_\ell + \text{Resid}\left(N_k^{n-1}\right) \tag{23}$$

where Δt_ℓ is the time-step size for the discrete phase, and $\text{Resid}\left(N_k^{n-1}\right)$ is the residual carried over from the previous time-level of droplet injection.

The charge carried by each droplet is calculated using

$$q_j = \bar{q}\left(\frac{d_{\ell,j}}{\bar{d}_\ell}\right)^\alpha \tag{24}$$

where $\bar{d}_\ell$ is the average diameter of the droplets. The charge carried by an average size droplet, $\bar{q}$, is obtained by dividing the measured total current by the number flow rate of average-sized droplets. According to the experimental work of Gomez and Tang [19], $\alpha \approx 2$ for d_ℓ smaller than approximately 50 μm, and $\alpha \approx 1.5$ for substantially larger droplets. Theoretical investigations on charge-to-mass ratio show that $\alpha \approx 1.5$ [20]. In the present work, $\alpha \approx 1.5$ is used following the work of Ganan-Calvo et al. [2].

4. Results

Two different cases of droplet dispersion are considered herein. In the first case,

calculations are made for dispersions of charged droplets occurring in a stagnant surrounding and the results are compared with available numerical results and measured data [1,2]. In the second case, dispersion of charged droplets coupled with fluid flow is calculated and the capability of the numerical method to solve droplet or particle dispersions occurring in laminar and turbulent flows is demonstrated. The calculated results are analyzed to investigate the trajectory of a droplet and the forces acting on the droplet. Physical data used in both calculations are described below.

The electrostatic spray emanating from a meniscus and the extent of the computational domain are shown schematically in Fig. 1. The length of the needle is 0.028 m, the inner radius (h) is 0.00025 m, and the outer radius is 0.00050 m. The distance between the meniscus and the collecting surface (H) is 0.0254 m. The other physical dimensions of the computational domain are: $a = 0.014\,m$, $b = 1.24H$, $c = H$, and $d = 0.95H$. The applied electric potential difference is 3040 *volts*, and the current carried by charged droplets is 4.3×10^{-8} *Ampere*. The liquid is heptane doped with an antistatic additive (STADIS 450, Du Pont). The liquid density is 685 Kg/m^3, and the volumetric flow rate is 2.3×10^{-9} m^3/sec. The measured data show that droplet diameters are distributed in between $35 \sim 50\ \mu m$ [2]. In the present work, the spray is represented by 5 different size groups with the diameters distributed between $\bar{d}_\ell - \sigma_s \bar{d}_\ell$ and $\bar{d}_\ell + \sigma_s \bar{d}_\ell$, where $\bar{d}_\ell = 40\ \mu m$ is the mean diameter and $\sigma_s = 0.20$ is the standard deviation. The number flow rate of each size droplet is calculated using the Gaussian distribution. In this case, the charge carried by an average-sized droplet is 6.26×10^{-13} *Coul*. The velocity of the liquid spray leaving the needle is 0.012 $m/$sec. The droplets are accelerated by the applied electric potential and by an air jet surrounding the needle [3]. However, detailed data for the air jet are not available. The annulus of the air jet is assumed to be 0.00025 m as shown in Fig. 1.

Dispersion of droplets in stagnant surrounding

The electrostatic spray emanating from a conical meniscus considered herein can be found in refs. [1,2]. Following the previous work [2], it is assumed that the airflow is negligibly small. The mesh for the entire domain and that near the injector are shown in Fig. 2.(a) and Fig. 2.(b), respectively. The smallest mesh size is $0.5\times10^{-4}m$ and the mesh away from the injector is stretched by a factor of 1.25. Note that the radius of the liquid injector is $0.25\times10^{-3}m$ while that for the collector surface is $0.254\times10^{-1}m$. The length scale of the injector is two orders of magnitude smaller than that of the entire domain as well as the droplet collector surface. The use of such a large stretch ratio is necessary to discretize a computational domain characterized by largely disparate length scales.

The boundary conditions for the electrical potential field are: $\phi = 3040\ volts$ for the meniscus, $\phi = 0$ along the surface of the droplet collector, and $\partial\phi/\partial n = 0$ along the center line and the entire external boundary. The air jet and air duct are treated as a free space so that the calculated potential field can be compared directly with the analytical and numerical results presented in ref. [2].

The calculated electrical potential field is shown in Fig. 3(a). The potential along the centerline obtained in the present study is in good comparison with analytical and numerical results [2] as shown in Fig. 3(b). The good comparison indicates that the present numerical method can resolve the highly steep and almost singular potential field near the meniscus. The calculated lines of force and the magnitude of force are shown in Figs. 3(c) and 3(d), respectively. Fig. 3(d) also shows that a strong electrical force field is concentrated in the region very close to the conical meniscus.

The number flow rate of average-sized droplets is calculated by dividing the volumetric flow rate of the conducting liquid by the volume of an average-sized

droplet, and the charge carried by an average-sized droplet is obtained by dividing the current by the number flow rate. Thus the number flow rate is inversely proportional to the cubic power of the droplet diameter, while the charge carried by an average-sized droplet is proportional to the cubic power of the diameter. The lines of force are closely aligned with the centerline in the spray region. Hence, the lateral dispersion of droplets is mostly caused by the Coulombic force acting among charged droplets and, hence, the calculated droplet dispersion in the radial direction depends strongly on the average droplet size. A few trial calculations revealed that the droplet dispersion also depends strongly on the mode of numerical droplet injection. The cause for such a dependence is discussed in the following "Two-phase flow with charged droplets" section. For the reasons discussed above, small uncertainties in measured current, volumetric flow rate, and the average droplet size can produce significantly different numerical results. To reduce uncertainty, the numerical droplets are seeded at $x = 0.012\,m$ in the present calculation. The lateral seed location is obtained using a random number generator, and the initial droplet velocity is obtained from measured data at the seed location. The time-step size for numerical integration of droplet equations of motion is $\Delta t_\ell = \Delta t_f / 100$, where $\Delta t_f = 0.175 \times 10^{-4}$ sec is the time-step size for the gas phase to be discussed in the following section. Calculations were also made using $\Delta t_\ell = \Delta t_f / 200$ to confirm the independence of the calculated results on the time-step size. The numerical results obtained using two different time-step sizes are practically identical. The initial droplet velocities and the calculated results at downstream locations are shown in Fig. 4. It can be found in the figure that the droplet velocity profiles obtained in the present study are in good agreement with the measured data. However, the present results exhibit wider later dispersion of droplets than those of ref. [2], and a few droplets disperse beyond $r = 0.01\,m$.

Two-phase flow with charged droplets

The inlet boundary of the air jet is located at the tip of the meniscus. The initial velocity of the air jet is 22 $m/\sec$ along the 45-degree inclined meniscus surface. The mesh and the applied electrical potential are the same as those described in the "Dispersion of droplets in stagnant surrounding" section. The time-step size for the fluid flow is $\Delta t_f = T_c / N_t$, where $T_c = 0.0035$ sec is a characteristic time for a droplet to reach the surface of the collector and $N_t = 200$ is the number of time-steps per characteristic time. The boundary conditions are as follows. At the upstream boundary above the air duct, $u = U_e$, $v = 0$, and a weak turbulence field is prescribed. Along the inclined surface of the liquid jet, the axial velocity of air is set equal to the liquid injection velocity, and $v = k_p = k_t = 0$ and $\partial \varepsilon_p / \partial n = \partial \varepsilon_t / \partial n = 0$. Along the center line and at the exit boundary, $v = 0$ and a vanishing gradient boundary condition is used for all other variables. At the external far field boundary, $u = U_e$, $v = 0$, and a vanishing gradient boundary condition is used for all other variables. Along the solid wall boundary of the droplet collecting surface, $u = v = k_p = k_t = 0$ and $\partial \varepsilon_p / \partial n = \partial \varepsilon_t / \partial n = 0$. External far fields are in a stagnant state in many EHD sprays. For the two-phase flow case considered in this section, more than 90 per cent of the domain is in a stagnant state. A stagnant state is certainly a trivial solution of the Navier-Stokes equations. However, numerically resolving such a stagnant state that extends through a large portion of the flow domain is not a trivial matter. To overcome numerical instability caused by the no fluid motion in a large extent of the domain, a small amount of free stream velocity, $U_e = 0.035 U_0$, has been used. Since the fluid flow and the particle dispersion occur in a small region along the center line, the external velocity does not significantly alter the two-phase fluid flow. Developing a numerical method to solve fluid flow occurring in a very small region of a large stagnant surrounding is a formidable task and it will be reported separately.

The calculated velocity vectors, pressure contours, and the turbulent kinetic energy contours for the gas-phase flow are shown in Figs. 5(a)~5(c), respectively. These figures show that a significant fluid motion occurs only in a narrow region along the center line. A very weak turbulence field is developed only along the air jet and the entire domain, including the center region, remains in a practically laminar state.

The convergence history for velocities, pressure, and conservation of mass is shown in Fig. 6(a) and that for turbulence variables is shown in Fig. 6(b). The L2 error norm for each flow variable is defined as

$$\|e(a)\| = \left[\sum_{i=2}^{n_x-1} \sum_{j=2}^{n_y-1} \left\{ \left(a_{i,j}^{new} - a_{i,j}^{old} \right) / \hat{a} \right\}^2 \Big/ (n_x - 2)(n_y - 2) \right]^{1/2} \tag{25}$$

where n_x and n_y are the number of grid points in the axial and radial directions, respectively, and $\hat{a} = \max\left\{ a_{i,j}^{new} | i = 2, n_x - 1 \; and \; j = 2, n_y - 1 \right\}$ is a normalizing factor. The global conservation of mass error is defined as

$$|e_{CM}| = (\dot{m}_{in} - \dot{m}_{out}) / \dot{m}_{in} \tag{26}$$

where $\dot{m}_{in}$ and $\dot{m}_{out}$ represent mass fluxes entering and leaving the domain, respectively. The small external velocity does not completely suppress the velocity and pressure wiggles. Yet, the present numerical method yields strongly convergent results as shown in these figures. It is shown in Fig. 6(b) that the multiple-time-scale turbulence equations yield strongly converged results for the weak turbulence field developing in a flow field with largely disparate length scales. The capability of the turbulence equations to accurately resolve complex transitional turbulence field can be found in ref. [11].

The droplets are seeded into the flow field after the flow field has reached a converged state. The droplet seed location confined within $\{(x,y)\,|\,0.0035 \le x \le 0.0042,\ 0. \le y \le 0.0007\}$ is calculated using a random number generator and the initial velocity of droplets is $5\ m/\sec$. As in the previous section, the use of $\Delta t_\ell = \Delta t_f / 100$ yields numerical results that are independent of the time-step size. The calculated streaklines are shown in Fig. 7. The convergence history for flow and turbulence variables are shown in Figs. 8(a) and 8(b), respectively. The number of droplets residing in the flow field versus time-level is shown in Fig. 8(c). As a steady state is approached, approximately 290 droplets exist in the flow field. For the two-phase flow case, the inter-phase momentum source term contributed by the discrete phase continuously disturbs the velocity field of the gas phase. To prevent accumulation of errors, the flow equations are solved iteratively for at least a prescribed number of iterations at each time-level. As shown in Figs 8(a) and 8(b), the use of 5 iterations per time-level let the flow and turbulence variables stay within a consistently converged state. After the prescribed minimum number of iterations is performed, calculations advance to a new time-level if either a prescribed convergence criterion is met or the number of iterations exceeds the prescribed maximum number of iterations. The convergence criterion used is $|e_{CM}| < 1.0 \times 10^{-3}$ and the maximum number of iterations is 25 per time-level.

The trajectory and velocity components of a droplet are shown in Fig. 9(a), and the axial and radial forces acting on the droplet are shown in Figs. 9(b) and 9(c), respectively. Immediately after the droplet is seeded, it is accelerated by the applied electrostatic force and aerodynamic force. Once the droplet attains its peak velocity, the aerodynamic force begins to decelerate the droplet. It can be found in Fig. 9(c) that the lateral dispersion of droplets is mostly caused by the Coulombic force. When a droplet is seeded at a relatively remote location from other droplets, the Coulombic force acting on the droplet is small. However, as soon as a new

droplet is seeded at a close location, the Coulombic force acting on the droplet is increased instantly. The dependence of droplet dispersion on the mode of numerical droplet seeding is caused by this phenomenon. As the particle travels toward the downstream direction, the Coulombic force becomes negligibly small due to the dispersion of droplets. At such downstream locations, a droplet can attain an equilibrium velocity that is balanced by the applied electrostatic force and the drag force.

5. Conclusions and discussion

A time-accurate numerical method to solve two-phase turbulent flows with charged particles or droplets in electrostatic field is presented. The method can solve dispersions of a discrete phase occurring in a stagnant surrounding, in laminar flows, and in turbulent flows. Therefore, the method can be used to investigate the dispersion of a charged discrete phase encountered in various engineering applications. The capability to analyze atomization of electrically conducting liquids is not included in this study. Atomization is an important , on-going, research subject by itself even for liquids that do not involve electrical force. The present method can be used advantageously for numerical investigation of such problems as spray painting and dust collecting mechanisms that do not involve atomization of electrically conducting liquids. For problems that involve atomization, such as aerosols, fabrication of solar panels, and the problem considered in the present study, the method provides limited capability to study dispersion of droplets that involve electrical force.

For the droplet dispersion occurring in a stagnant surrounding, the calculated droplet velocity profiles are in good agreement with the measured data. The calculated results obtained in the present study exhibit wider lateral dispersion than that obtained by Ganan-Calvo et al. [2]. The lateral dispersion is mostly caused by

the Coulombic force acting among charged droplets. It is shown that the Coulombic force depends strongly on the charge carried by each droplet and the mode of numerical droplet injection. In ref. [2] and here, the charge carried by an average-sized droplet is calculated by dividing the current by the number flow rate of droplets. The number flow rate is inversely proportional to the cubic power of the average droplet diameter. Hence a small uncertainty in the measured droplet size, current, and volumetric flow rate can cause a substantial difference in calculated results.

For the flow case considered in this study, a large extent of the domain is in a nearly stagnant state. It is found that the large stagnant surrounding causes numerical instability. Introducing a small external velocity suppresses the numerical instability and yields strongly convergent and physically correct results. A weak turbulence field is developed only near the exit of the air jet and the entire flow field remains in an almost laminar state. It is shown that the multiple-time-scale turbulence equations do not cause difficulty in obtaining a highly convergent result. In fact, the turbulence equations yield strongly converged results for the weak turbulence field developing in a flow field with largely disparate length scales. Comparisons of the aerodynamic force, electrostatic force caused by the applied electrical field, and the Coulombic force acting on a charged droplet help to better understand the characteristics of dispersion of charged particles or droplets occurring in two-phase flows. Measured data for two-phase flows with a charged discrete phase are very scarce, and more detailed measured data are certainly necessary for further improvement and verification of numerical methods to solve two-phase flows with a charged discrete phase.

A few difficulties in numerical simulations of two-phase flows with a charged discrete phase are discussed below. Usually, the time-step size of the discrete phase in two-phase flows needs to be by far smaller than that for the gas phase in order to

obtain numerical results that are independent of the time-step size used. Otherwise, the inter-phase momentum transfer may not be resolved correctly. The time-step size of the discrete phase for two-phase flows with charged droplets needs to be even smaller than that without Coulombic force. If the time-step size for the discrete phase is not sufficiently small, then droplets can approach infinitely close to each other and these droplets may be subjected to a large Coulomb force since the Coulomb force between charged droplets is inversely proportional to the square of the distance between the droplets. In such a case, a large Coulomb force accelerates droplets so greatly that an unphysically large inter-phase momentum transfer rate can be produced and the numerical method for the gas-phase may fail to yield a converged solution. Only the use of a very small time-step size can yield a physically correct droplet distribution pattern.

References

1. Barrero, A., and Rumeau, E., "Estudio experimental de la atomizacion electrodinamica de liquidos," Research Report, E. T. S. I. I., Universidad de Sevilla, Sevilla, Spain, 1992.
2. Ganan-Calvo, A. M., Lasheras, J. C., Davila, J., and Barrero, A., "The electrostatic spray emitted from an electrified conical meniscus," *J. Aerosol Sci.,* vol. 25, no. 6, pp. 1121-1142, 1994.
3. Ganan-Calvo, A. M., *Private communication,* February, 1995.
4. Gomez, A., and Chen, G., "Charged-induced secondary atomization in diffusion flames of electrostatic spray," *Combust. Sci. and Tech.,* vol. 96, pp. 47-59, 1994.
5. Crowe, C. T., Sharma, M. P., and Stock, D. E., "The particle-source-in-cell (PSI-CELL) model for gas-droplet flows," *J. Fluid Engr.,* pp. 325-332, 1977.
6. Kim, S.-W., and Benson, T. J., "Comparison of the SMAC, PISO and Iterative Time-Advancing Schemes for Unsteady Flows," *Computers and Fluids*, vol. 21, no. 3, pp. 435-454, 1992.
7. Kim, S.-W., "Calculations of Separated 3-D Flows with a Pressure-Staggered Navier-Stokes Equations Solver," NASA CR-187065, 1991.
8. Kim, S.-W., "Numerical investigation of chemical reaction - turbulence interaction in compressible shear layers," *Combustion & Flame,* vol. 101, pp. 197-208, 1995.
9. Kim, S.-W., and Benson, "Fluid flow of a row of jets in crossflow - A numerical study," T. J., *AIAA J.* 31:806-811, 1993.
10. Kim, S.-W., and Benson, T. J., "Calculation of a circular jet in crossflow with a multiple-time-scale turbulence model," *Int. J. Heat Mass Transfer*, 35:2357-2365, 1992.
11. Kim, S.-W., Zaman, K. B. M. Q., and Panda, "Numerical investigation of

unsteady transitional flow over oscillating airfoil," ASME *J. Fluid Engineering,* vol. 117, pp. 10-16, 1995.

12. Tavoularis, S., and Karnik, U., "Further experiments on the evolution of turbulent stresses and scales in uniformly sheared turbulence," *Journal of Fluid Mechanics*, Vol. 204, pp. 457-478, 1989.
13. Launder, B. E., "A Generalized Algebraic Stress Transport Hypothesis," *AIAA J.*, Vol. 20, pp. 436-437, 1982.
14. Rodi, W., "The Prediction of Free Boundary Layers by Use of a Two-Equation Model of Turbulence," Ph.D. Thesis, University of London, London, 1972.
15. Faeth, G. M., "Current status of droplet and liquid combustion," *Prog. Energy Combust Sci.,* vol. 3, pp. 191-224, 1977.
16. El Banhawy, Y., and Whitelaw, J. H., "Calculation of the flow properties of a confined kerosene-spray flame," *AIAA J.,* vol. 18, no. 12, pp. 1503-1510, 1980.
17. Raju, M. S., and Sirignano, W. A., "Multicomponent spray computations in a modified centerbody combustor," *J. Propulsion,* vol. 6, no. 2, pp. 97-105, 1990.
18. Panofsky, W. K., and Phillips, M., *Classical electricity and magnetism,* Addison-Wesley Publishing Co., Menlo Park, California, 1962.

19 Gomez, A., and Tang, K., "Charge and fission of droplets in electrostatic sprays," *Physics of Fluids*, vol. 6, pp. 404-414, 1994.

20. Pfeifer, R. J., and Hendricks, C. D., "Charge-to-mass relationships for electrohydrodynamically sprayed liquid droplets," Physics of Fluids, pp. 2149-2154, 1967.

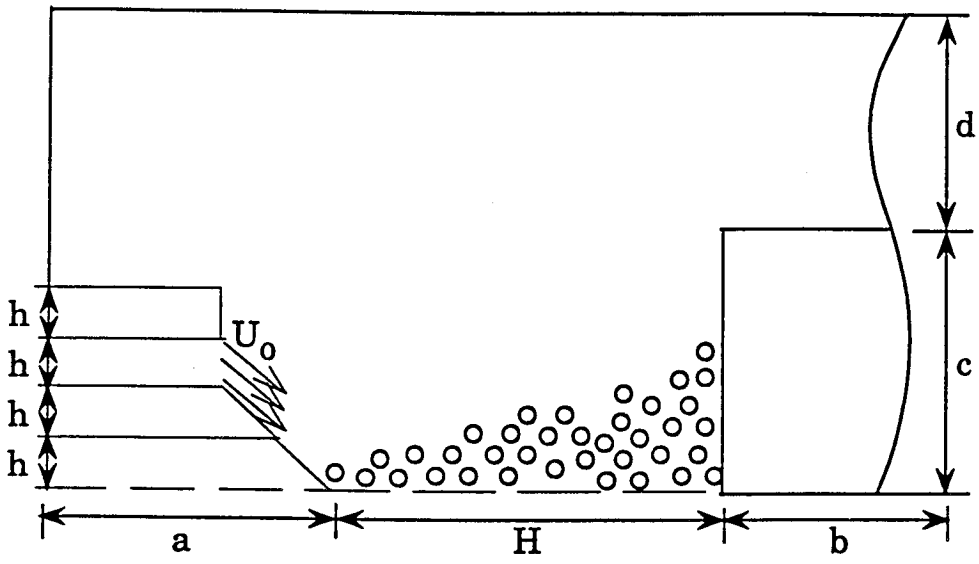

1. Nomenclature and computational domain for EHD spray.

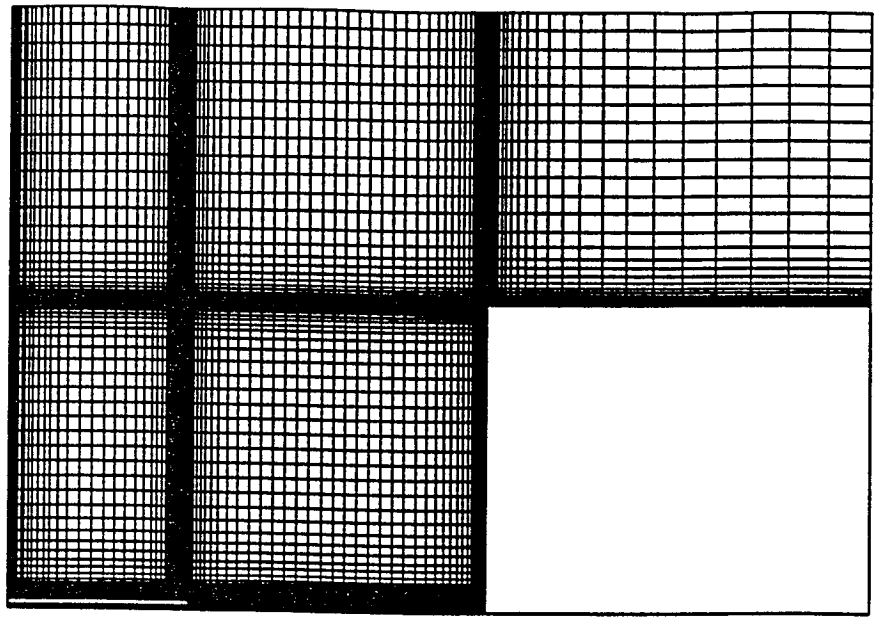

(a) mesh for entire domain,

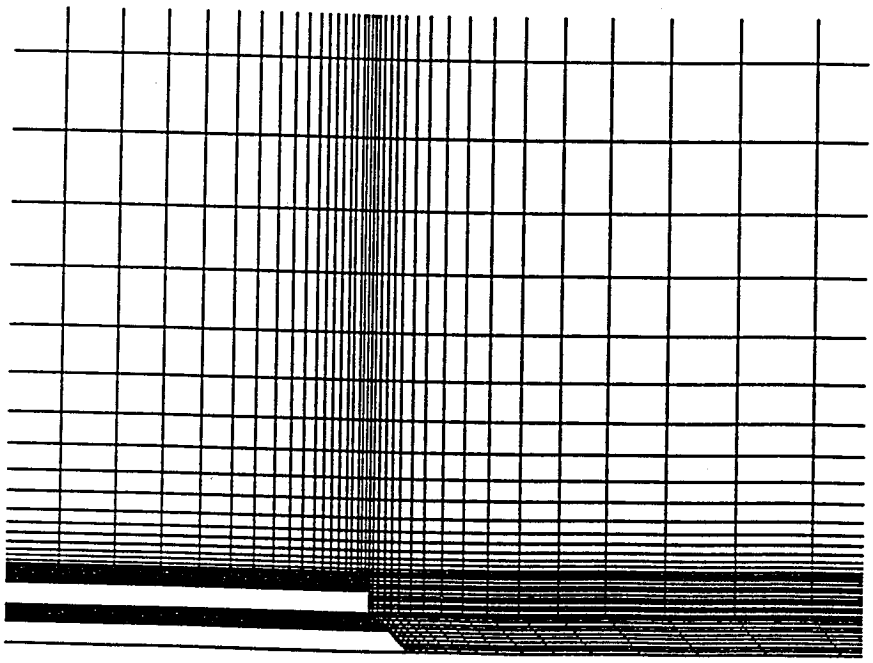

(b) mesh near injector.

2. 109×87 Mesh,

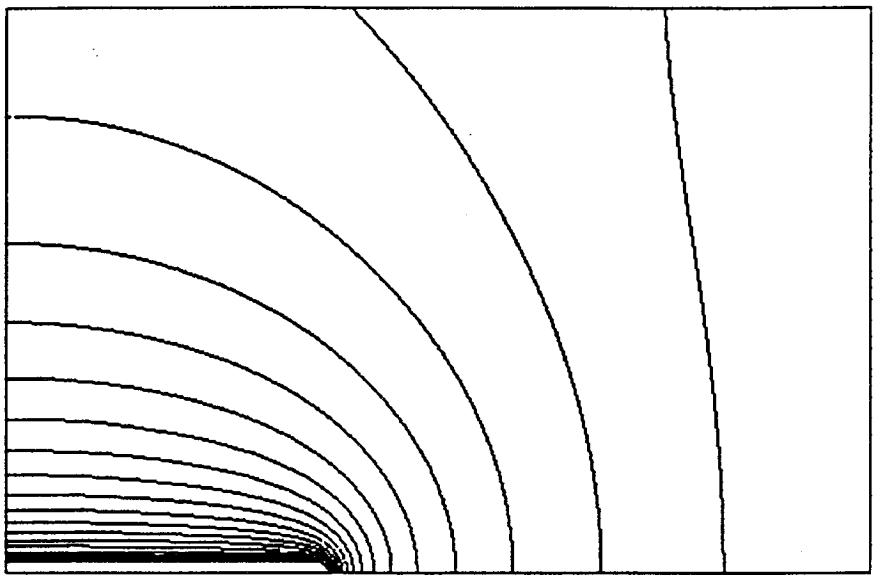

(a) contour plot, $0 \le \phi \le 3040$ *volts*, and $\Delta\phi = 160$

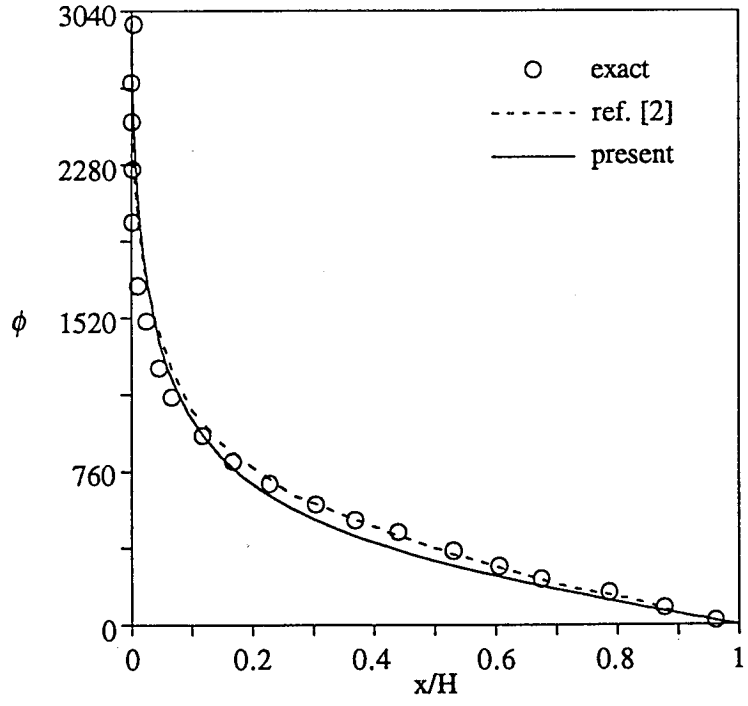

(b) Comparisons of calculated electrostatic fields,

3. Applied electrostatic potential field

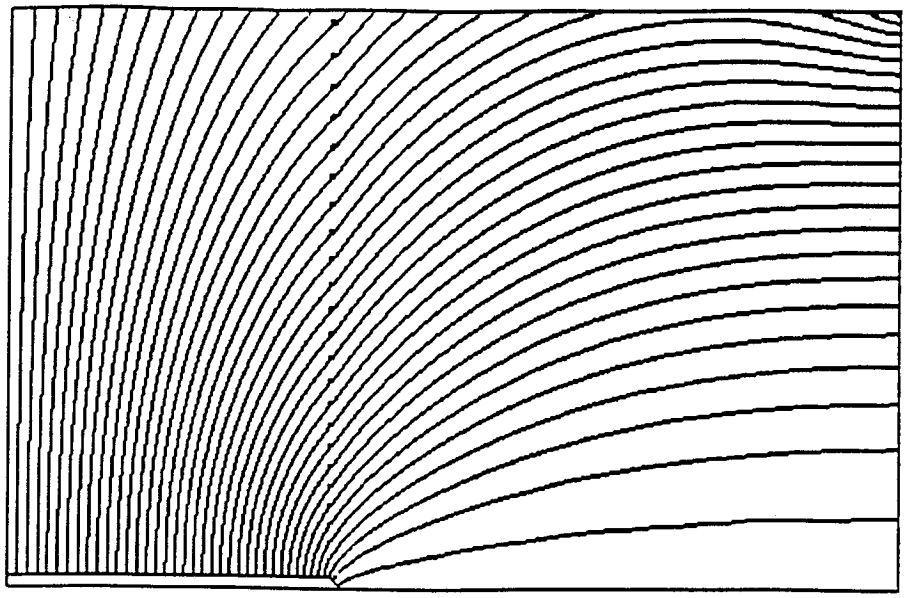

(c) Lines of force,

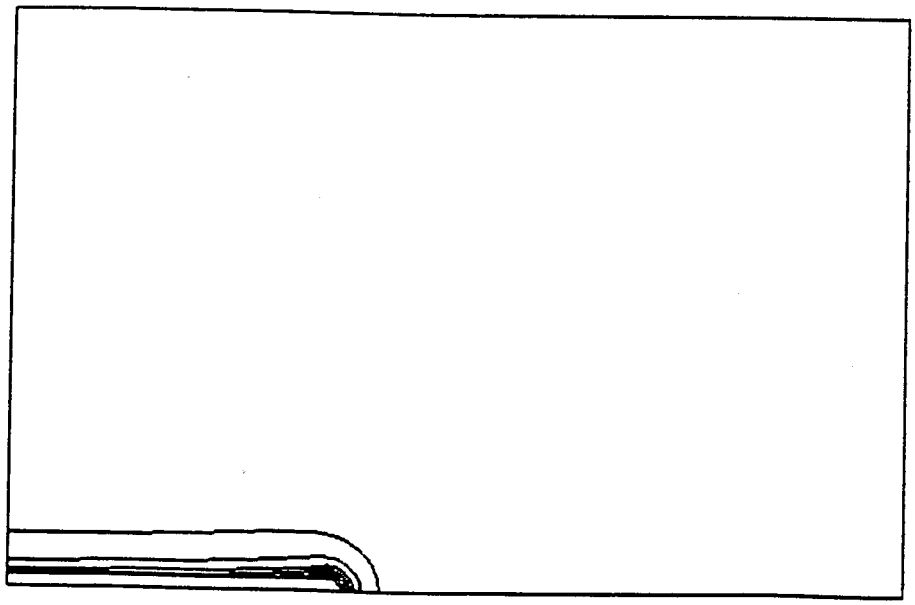

(d) Magnitude of force, $0 \le |\nabla\phi| \le 6.263 \times 10^6$, and $\Delta|\nabla\phi| = 3.132 \times 10^5$.

Figure 3 - Continued,

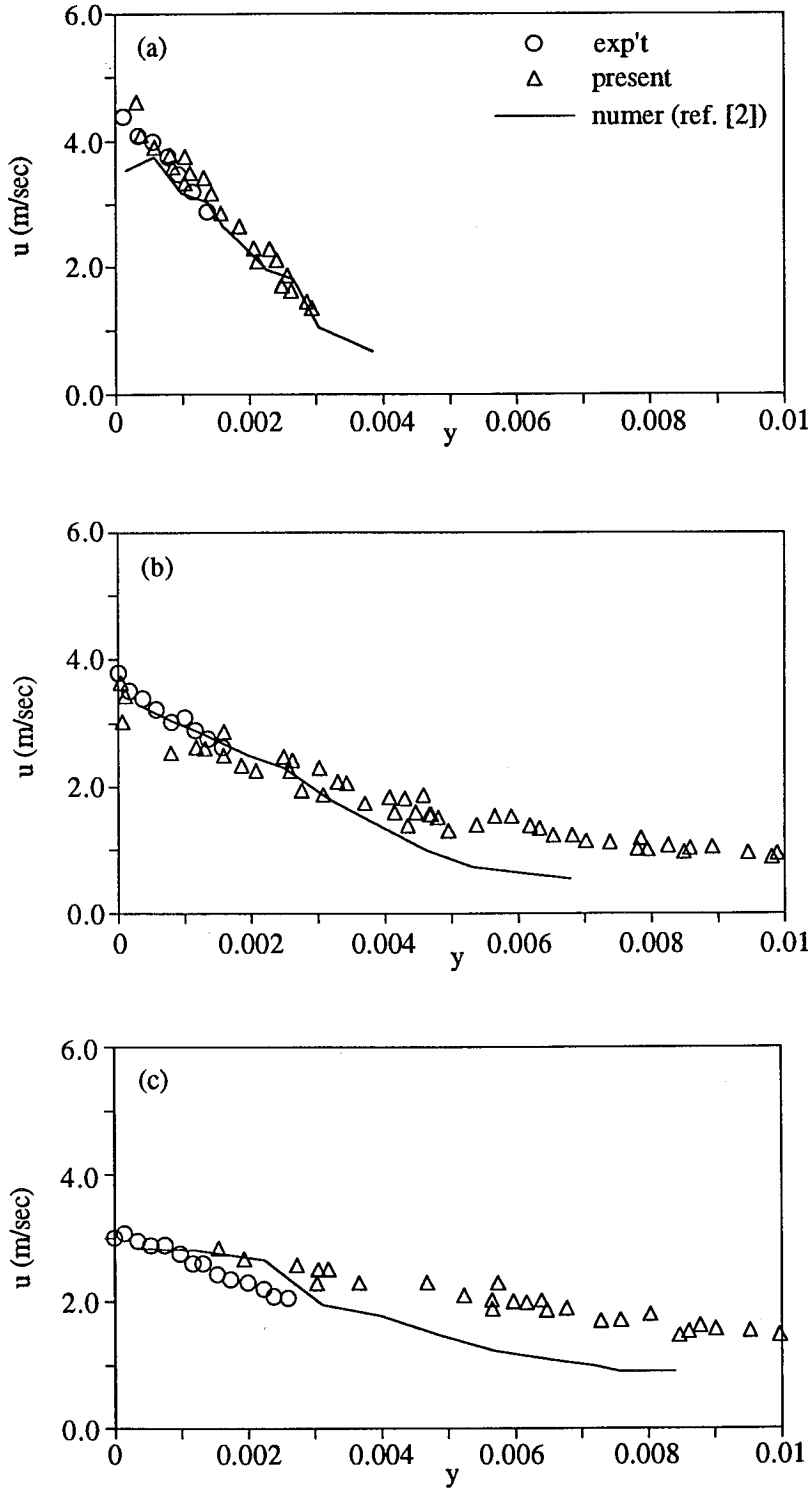

4. Dispersion of charged droplets in stagnant surrounding, (a) at x=0.012 *m*, (b) at x=0.017 *m*, (c) at x=0.022 *m*.

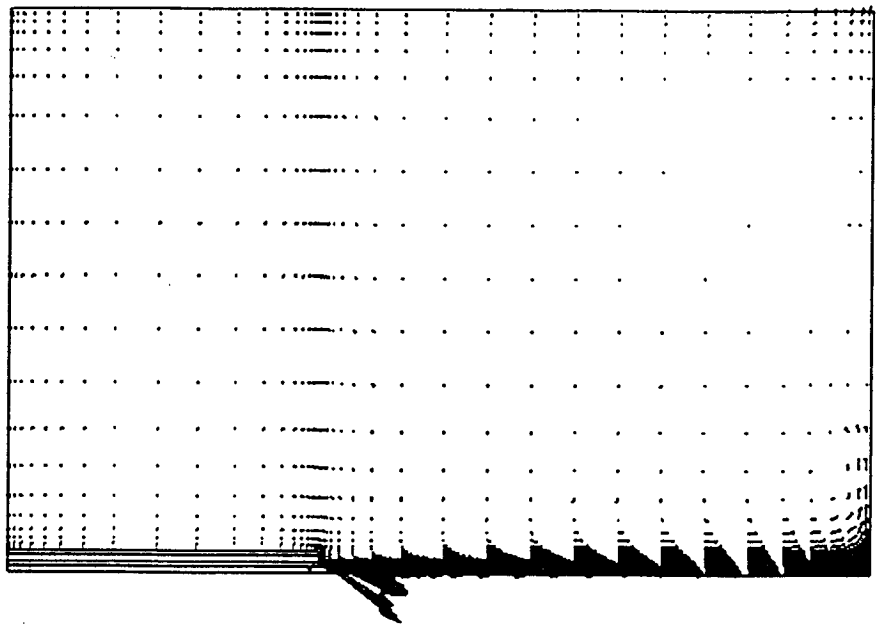

(a) velocity vectors, $0 \le |\mathbf{V}| \le 22 \ \ m/\text{sec}$,

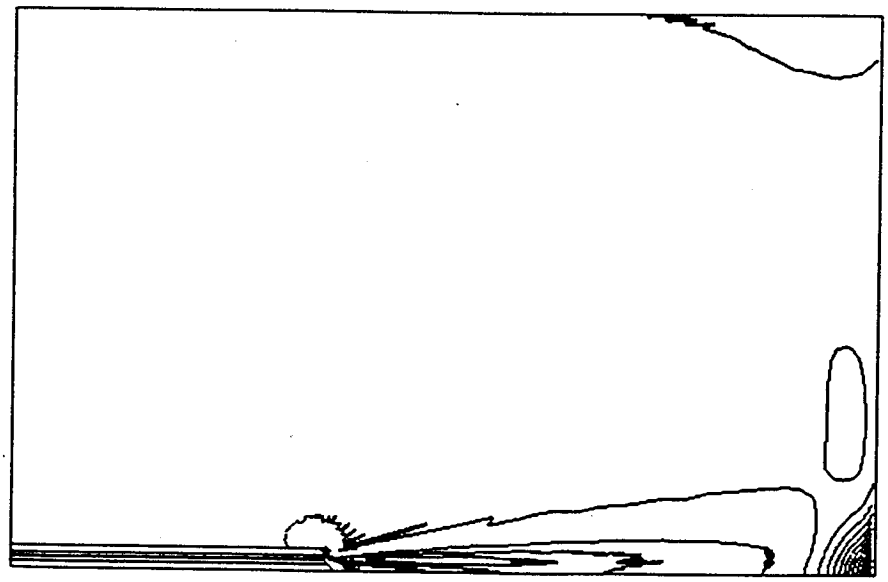

(b) pressure contours, $-10 \le p \le 20 \ \ Newton/m^2$, $\Delta p = 1.50$,

5. Calculated flow field

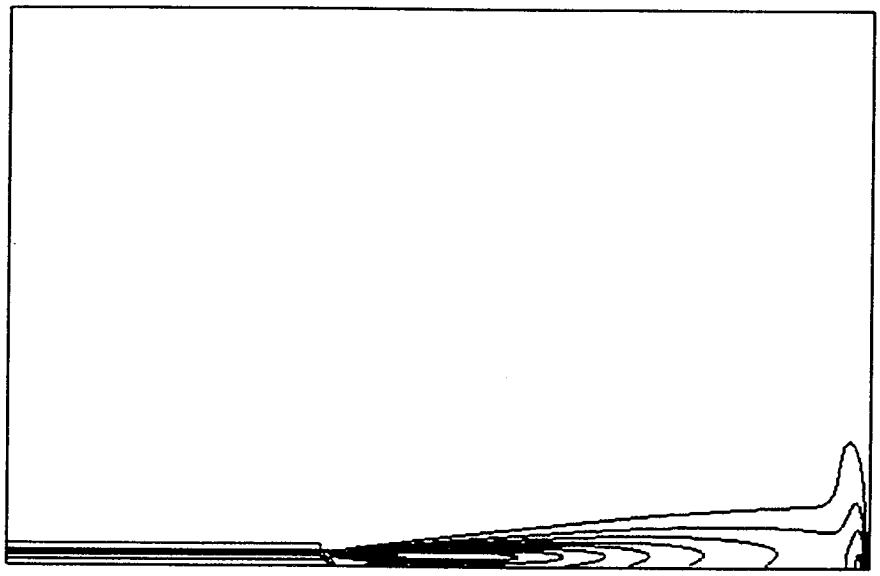

(c) turbulent kinetic energy contours, $0 \le k \le 8\ m^2/\sec^2,\ \Delta k = 0.8.$

Figure 5 - continued.

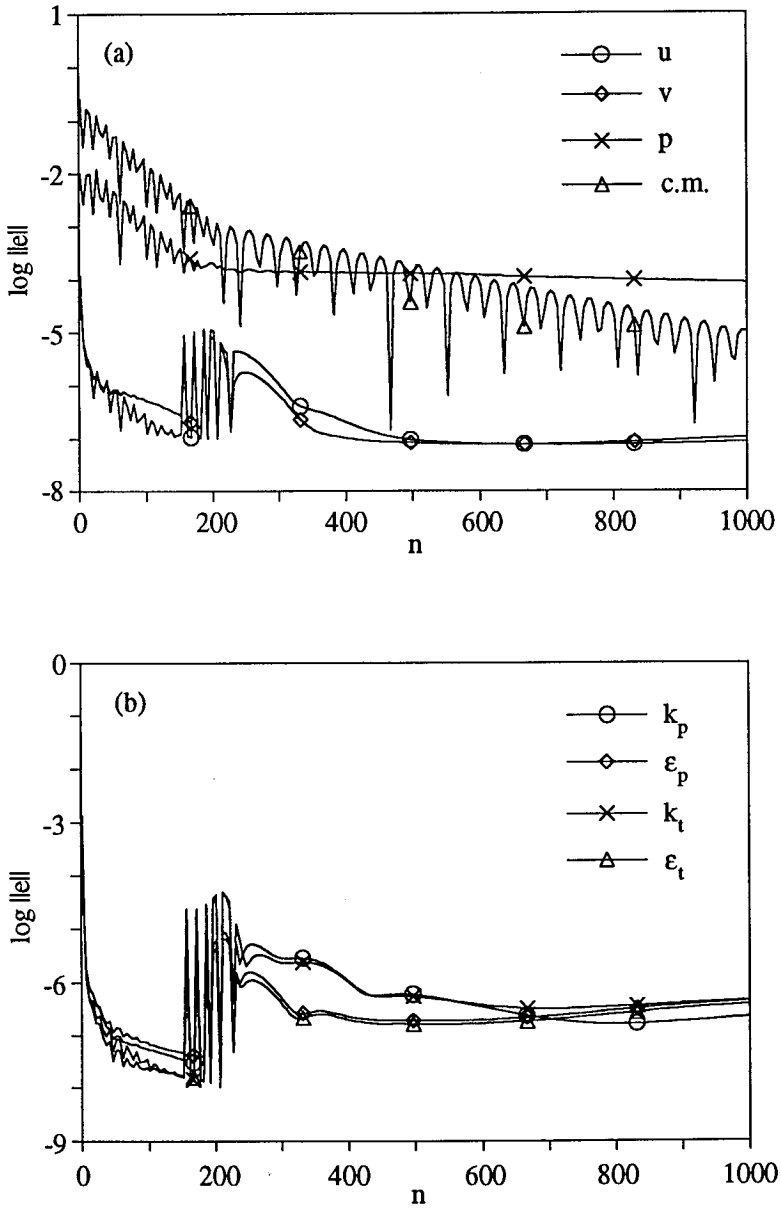

6. Convergence history for fluid flow,
(a) flow variables, (b) turbulence variables.

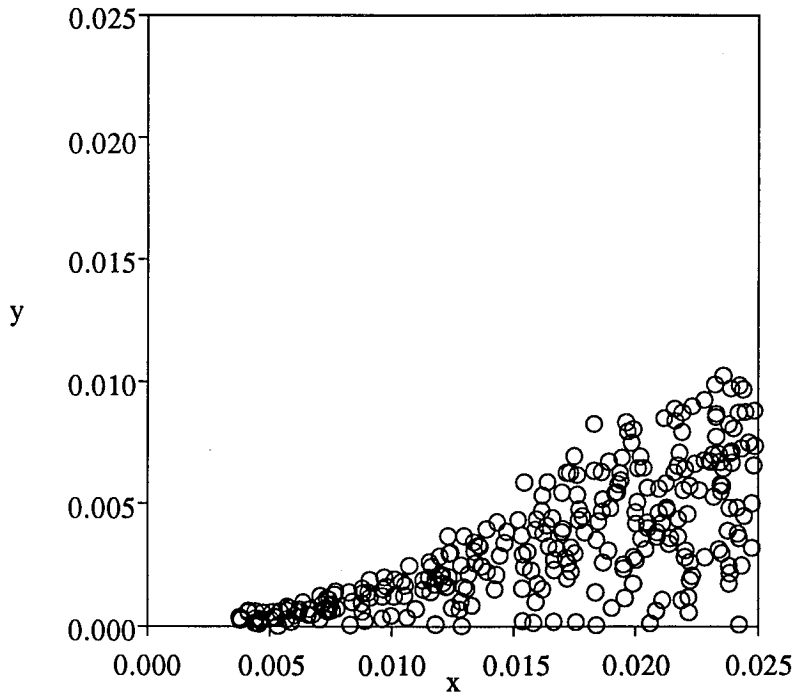

7. Dispersion of charged droplets in turbulent flow

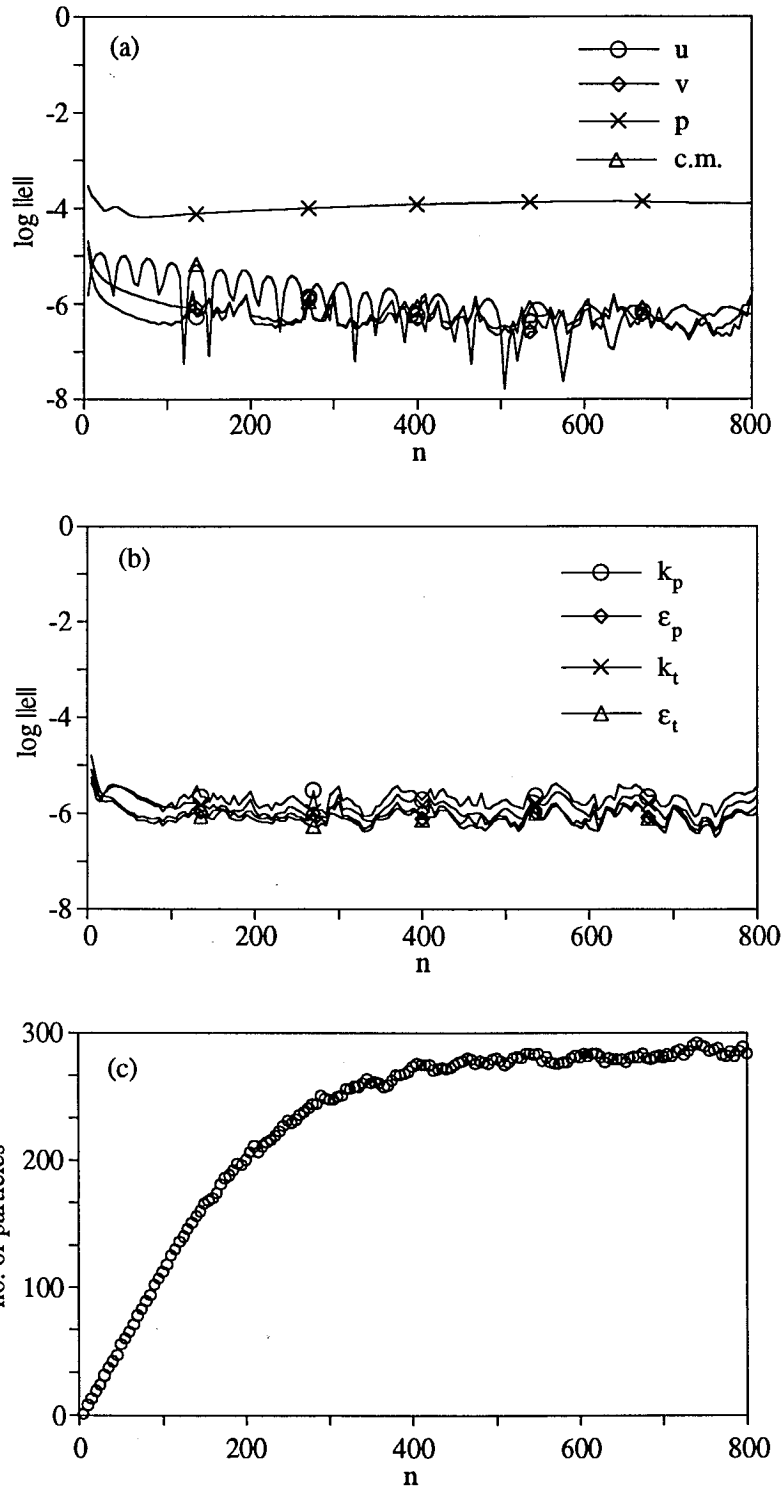

8. Convergence history for two-phase flow,
(a) flow variables, (b) turbulence variables, (c) number of droplets.

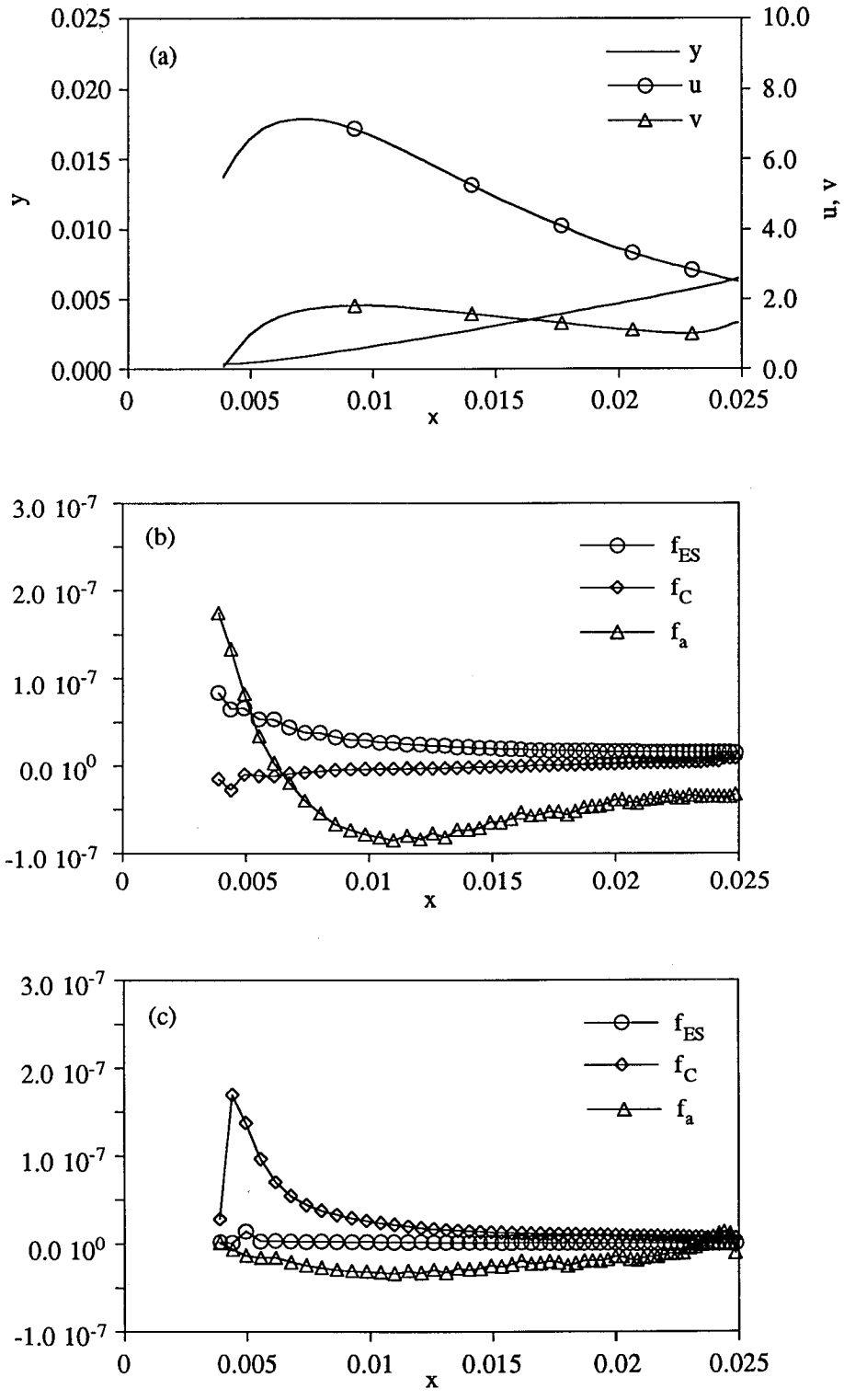

9. Droplet trajectory, velocity, and force acting on a droplet, (a) trajectory and velocity, (b) axial force, and (c) radial force.

REPORT DOCUMENTATION PAGE

Form Approved
OMB No. 0704-0188

1. AGENCY USE ONLY (*Leave blank*)	2. REPORT DATE	3. REPORT TYPE AND DATES COVERED
	February 1996	Final Contractor Report

4. TITLE AND SUBTITLE

Numerical Investigation of Two-Phase Flows with Charged Droplets in Electrostatic Field

5. FUNDING NUMBERS

WU–243–30–07
C–[redacted]–78048–D

6. AUTHOR(S)

Sang–Wook Kim

7. PERFORMING ORGANIZATION NAME(S) AND ADDRESS(ES)

Thermoscience Research Corporation
2001 Aerospace Parkway
Brook Park, Ohio 44142

8. PERFORMING ORGANIZATION REPORT NUMBER

E–10110

9. SPONSORING/MONITORING AGENCY NAME(S) AND ADDRESS(ES)

National Aeronautics and Space Administration
Lewis Research Center
Cleveland, Ohio 44135–3191

10. SPONSORING/MONITORING AGENCY REPORT NUMBER

NASA CR–198452

11. SUPPLEMENTARY NOTES

Project Manager, Robert Stubbs, Internal Fluid Mechanics Division, NASA Lewis Research Center, organization code 2670, (216) 433–6303.

12a. DISTRIBUTION/AVAILABILITY STATEMENT

Unclassified - Unlimited
Subject Category 34

This publication is available from the NASA Center for Aerospace Information, (301) 621–0390.

12b. DISTRIBUTION CODE

13. ABSTRACT (*Maximum 200 words*)

A numerical method to solve two-phase turbulent flows with charged droplets in electrostatic field is presented. The ensemble-averaged Navier-Stokes equations and the electrostatic potential equation are solved using a finite volume method. The transitional turbulence field is described using multiple-time-scale turbulence equations. The equations of motion of droplets are solved using a Lagrangian particle tracking scheme, and the inter-phase momentum exchange is described by the Particle-In-Cell scheme. The electrostatic force caused by an applied electrical potential is calculated using the electrostatic field obtained by solving a Laplacian equation and the force exerted by charged droplets is calculated using the Coulombic force equation. The method is applied to solve electro-hydrodynamic sprays. The calculated droplet velocity distributions for droplet dispersions occurring in a stagnant surrounding are in good agreement with the measured data. For droplet dispersions occurring in a two-phase flow, the droplet trajectories are influenced by aerodynamic forces, the Coulombic force, and the applied electrostatic potential field.

14. SUBJECT TERMS	15. NUMBER OF PAGES
Two-phase flows; Turbulence; Electrostatic potentials; Navier-Stokes equations	40
	16. PRICE CODE: A03

17. SECURITY CLASSIFICATION OF REPORT	18. SECURITY CLASSIFICATION OF THIS PAGE	19. SECURITY CLASSIFICATION OF ABSTRACT	20. LIMITATION OF ABSTRACT
Unclassified	Unclassified	Unclassified	

National Aeronautics and
Space Administration

Lewis Research Center
21000 Brookpark Rd.
Cleveland, OH 44135-3191